

1 The format of this reply to C. van Heerwaarden (referee) is as follows:

2

3 In the first part, "**Authors' Response to C. van Heerwaarden**", we provide  
4 a point-by-point response to the referee's comments. We provide each of the referee's  
5 comments in **bold font**. After each comment that requires a response we provide a  
6 response (in regular font). If we modified the manuscript in response to a comment, we  
7 describe what the modification was, and indicate where it was made in the revised  
8 manuscript (the revised manuscript is provided at the end of the document).

9

10 In the second section, **Additional modifications to the manuscript**, we  
11 describe modifications to the manuscript not made in response to any specific comment  
12 of either referee. For the most part these modifications are minor, however we did fix  
13 two errors in the final analytical solution (errors in the text, not the code; so these did  
14 not affect any of the presented results).

15

16 In the third section, we provide the revised manuscript.

17

18 Authors' Response to Referee C. van Heerwaarden (Referee)

19

20 **General comments**

21 **I recommend minor revisions. The paper presents a validation test for solvers for buoyancy**  
22 **driven flows. To the reviewer's knowledge it is the first validation test for wall-bounded**  
23 **Boussinesq flows including buoyancy and therefore deserves publishing. I have tested the**  
24 **MicroHH (<http://github.com/microhh/microhh>) code against the analytical solution**  
25 **provided in the paper and it gives the correct solutions (see attached figures). Nonetheless,**  
26 **there are a couple of improvements that could be made. First of all, it would be great if the**  
27 **reference cases could be presented in a non-dimensional framework, to make them more**  
28 **general. Second, GMD suggests strongly to submit code for benchmarking papers. I would**  
29 **appreciate if the authors can provide their code, to enable the readers to use the test case**  
30 **with their own code.**

31 We probably should have started the project in non-dimensional form, but since we did  
32 not, we are hesitant to recast the theory and code into non-dimensional forms. The changes,  
33 while straightforward for both the text and code, would be extensive and thus offer new  
34 possibilities for errors to creep in.

35 Yes, we agree that the test code should be freely available. The Fortran code for the  
36 analytical solution is now included as a supplement to the article. The code is named "square.f"  
37 ("square" because the disturbance is a square wave) and it is configured for Test 1-A. A  
38 statement on code availability has been added just before the Acknowledgements statement.

39

40 **Abstract Maybe the authors can stress here that there are very few, or maybe even no**  
41 **analytical solutions for wall-bounded buoyancy driven flows around and their paper is**  
42 **therefore really a novelty.**

43 In the abstract we have added the sentence: "The analytical solution is one of the  
44 few available for wall-bounded buoyancy-driven flows."

45

46 **Page 2850 Can the authors shortly explain how they got to their set of equations?**

47 We have added a few lines describing the individual governing equations. We

48 also give a reference for the equations (Chandrasekhar 1961) and for the Brunt-Väisälä  
49 frequency  $N$  that appears in the thermal energy equation (Kundu 1990).

50

51 **Page 2857 It would be good if the authors can write some guidelines on how to use their**  
52 **validation test with a model with staggered grids. For instance, if  $\mathbf{u}$  is interpolated, how fine**  
53 **does the analytical solution need to be in order to have reference data for which the error**  
54 **in the analytical solution is negligible to the model error?**

55 The analytical solution can easily be output to a staggered grid. If one is coding  
56 the analytical solution from scratch (i.e., not using our computer code), one can input  $x$   
57 and  $z$  locations that coincide with the staggered points. One can use a different set of  $x$   
58 and  $z$  locations for any of the dependent variables. Our current computer code for the  
59 analytical solution is set up to use the same  $x$  and  $z$  locations for all variables (i.e.,  
60 unstaggered arrangement), but it is straightforward to modify that code so the  
61 dependent variables are output on any desired grid.

62

63 **Formula 41 Why don't the authors define the first Reynolds number as the vorticity**  
64 **advection divided by the vorticity diffusion?**

65 Actually, in a continuum sense, since  $\frac{\partial b}{\partial x} = \nu \nabla^2 \eta$  (from equation (2.5)), our

66 definition  $R_\eta \equiv \frac{\max |\mathbf{u} \cdot \nabla \eta|}{\max |\partial b / \partial x|}$  is equivalent to the definition suggested by the referee,

67  $R_\eta \equiv \frac{\max |\mathbf{u} \cdot \nabla \eta|}{\max |\nu \nabla^2 \eta|}$ . In practice, however, the errors associated with discretizing  $\nabla^2 \eta$  may

68 be worse than those associated with discretizing  $\partial b / \partial x$ , so we prefer our definition.

69

70 **Page 2859 Why are 50.000 terms taken? Isn't this an enormous amount?**

71 Yes, for the two test cases presented the 50000 terms is an enormous amount.  
72 However, in the course of the testing (we only showed two tests, but have conducted

73 many additional tests, including tests over larger horizontal domains), we did not want  
74 to be burdened by having to go back and rerun a test in case we had too few terms. By  
75 choosing such a large number, we removed that parameter from further consideration.

76

77 **Page 2864 Do I understand correctly that the authors underline statements by previous**  
78 **papers that models on a staggered grid do not require a pressure boundary condition?**

79 We were trying to be diplomatic in our statements on that page, and believe that the  
80 current phrasing in the original manuscript is accurate, but we do not want to make too much out  
81 of it. In going through both engineering and meteorological modeling literature, we were struck  
82 at how often key details related to the pressure boundary condition were glossed over or omitted.  
83 In many cases it was not possible to determine what was actually implemented.

84

85 **Page 2865 In the last statement the authors mention the numerical boundary layers. Are**  
86 **these a problem in explicit codes as they are using as well, or does this problem only play a**  
87 **role in case implicit diffusion has to be applied?**

88 We did not observe the development of thin numerical boundary layers in any of our  
89 tests. However, we don't know whether this is because our code is explicit or is related to the  
90 nature of the test flows we considered. The thin numerical boundary layers reported in the  
91 literature have generally been for test flows dominated by advection rather than diffusion.

92

93 **Figure 6 Why are the results asymmetric? You are solving a purely symmetric system.**  
94 **Which process introduces the asymmetry in the solution?**

95 The asymmetry is a result of nonlinearities in the numerically simulated flow. By  
96 the time the numerical solution has evolved to the point shown in Figure 6, the flow is  
97 no longer in a linear regime. If we consider the motion in one convective cell we have an  
98 ascending warm branch and a descending cooler branch, which would be symmetric if  
99 the system remained linear (and of course it is linear/symmetric in the analytical test  
100 case). However, in the numerically simulated flow, the (positive) buoyancy in the rising  
101 branch is transported laterally (nonlinear advection) at the top of the circulation cell to  
102 the top of the descending cell. This introduces an asymmetry to the circulation. Once

103 the symmetry of the flow is broken, the flow can become quite complicated.

104

105 Additional modifications to the manuscript (i.e., not made in  
106 response to the reviewers' comments)

107

108 Please note that the third author would like his middle initial "A" included in his name:  
109 Jeremy A. Gibbs.

110

111 We have added a new reference: Egger (1981). The Egger study was related to ours in  
112 that it was concerned with a linear analysis of the 2D Boussinesq governing equations  
113 for thermally driven flow. Egger's analysis was largely for slope flows, though with flat  
114 terrain (our focus) considered as a special case. However, Egger outlines how to get the  
115 analytical solution but does not actually provide the final analytical solution. We  
116 mention this Egger study in the second paragraph of Section 1. We also mention it in  
117 the paragraph right after (2.8): the restriction on acceptable surface buoyancies  
118 described in that paragraph was first noted by Egger, though without details.

119

120 A correction was made to the original equations (2.39) and (2.40) [these now appear as  
121 equations (2.40) and (2.42), respectively]. The factor  $k^{1/3}$  in the denominator of the  
122 term in front of the summation in (2.39) and the factor  $k^{2/3}$  in the numerator of the  
123 term in front of the summation in (2.40) should be kept inside the summations. These  
124 factors were treated correctly in the computer code, so none of the presented results  
125 were affected.

126

127 Section 3. We now make the number of points in the  $x$  and  $z$  direction unambiguous:  
128 instead of writing the number of points in test A-1 as (513, 1025) we write, "...consisted  
129 of 513 points in the  $x$  direction and 1025 points in the  $z$  direction,..." Similarly, for test  
130 A-2, we now write, "...was generated with 2049 points in the  $x$  direction and 513 points

131 in the  $z$  direction,..."

132

133 In the Appendix we now write the time step as  $\Delta t$  instead of  $\delta t$  since the symbol  $\delta$   
134 has already been used to represent the divergence of the velocity field.

135

136 In several places in the manuscript we now use bold to indicate the vector  $\mathbf{u}$  (formerly  
137 we used  $\vec{u}$ ).

138

139 We have slightly modified the acknowledgements statement (we now thank the  
140 anonymous reviewer).

141

142        **An analytical verification test for numerically simulated convective flow**

143                                **above a thermally heterogeneous surface**

144                                by Alan Shapiro, Evgeni Fedorovich, and Jeremy A. Gibbs

145

146    **Abstract.** An analytical solution of the Boussinesq equations for the motion of a  
147    viscous stably stratified fluid driven by a surface thermal forcing with large horizontal  
148    gradients (step changes) is obtained. This analytical solution is one of the few available  
149    for wall-bounded buoyancy-driven flows. The solution can be used to verify that  
150    computer codes for Boussinesq fluid system simulations are free of errors in formulation  
151    of wall boundary conditions and to evaluate the relative performances of competing  
152    numerical algorithms. Because the solution pertains to flows driven by a surface thermal  
153    forcing, one of its main applications may be for testing the no-slip, impermeable wall  
154    boundary conditions for the pressure Poisson equation. Examples of such tests are  
155    presented.



## 156 1 Introduction

157 Thermal disturbances associated with variations in underlying surface properties can  
158 drive local circulations in the atmospheric boundary layer (Atkinson, 1981; Briggs, 1988;  
159 Hadfield et al., 1991; Segal and Arritt, 1992; Simpson, 1994; Mahrt et al., 1994; Pielke,  
160 2001; McPherson, 2007; Kang et al., 2012) and affect the development of the convective  
161 boundary layer (Patton et al., 2005; van Heerwaarden et al., 2014). Computational fluid  
162 dynamics (CFD) codes for modeling such flows commonly solve the Boussinesq  
163 equations of motion and thermal energy for a viscous/diffusive stably stratified fluid. In  
164 this paper we present an analytical solution of the Boussinesq equations for flows driven  
165 by a surface thermal forcing with large gradients (step changes) in the horizontal. The  
166 solution can be used to verify that CFD codes for Boussinesq fluid system simulations  
167 are free of errors, and to evaluate the relative performances of competing numerical  
168 algorithms. Such verification procedures are important in the development of CFD  
169 models designed for research, operational, and classroom applications.

170 We solve the linearized Navier-Stokes and thermal energy equations analytically  
171 for the case where the surface buoyancy varies laterally as a square wave (Fig. 1).  
172 Attention is restricted to the steady state. No boundary-layer approximations are made;  
173 the solution is non-hydrostatic, and both horizontal and vertical derivatives are included  
174 in the viscous stress and thermal diffusion terms. The solution is similar to that of  
175 Axelsen et al. (2010) for katabatic flow above a cold strip, but is easier to evaluate (no

176 slope present) and applies to the more general scenario where the viscosity and  
177 diffusivity coefficients can differ. The flow is also similar to a special case (no slope)  
178 considered by Egger (1981), although a final analytical solution was not provided in  
179 that study. Strictly speaking, the linearized Navier-Stokes equations apply to a class of  
180 very low Reynolds number motions known as creeping flows. Such flows appear in  
181 studies of lubrication, locomotion of microorganisms, lava flow, and flow in porous  
182 media. Of course, for the task at hand, if our linear solution is to serve as a benchmark  
183 for a nonlinear numerical model solution, it is essential that the parameter space be  
184 restricted to values for which the model's nonlinear terms are negligible.

185         Because the solution pertains to flows driven by a surface thermal forcing, one of  
186 its main applications may be as a test for surface boundary conditions in the pressure  
187 Poisson equation. In models of atmospheric boundary layer flows, the buoyancy is a  
188 major contributor to the forcing term in the Poisson equation and also appears in the  
189 associated surface boundary condition. The pressure boundary condition on a solid  
190 boundary in incompressible (Boussinesq) fluid flows is an important and complex issue  
191 that has long been fraught with technical difficulties and controversies (Strikwerda,  
192 1984; Orszag et al., 1986; Gresho and Sani, 1987; Gresho, 1990; Temam, 1991; Henshaw,  
193 1994; Petersson, 2001; Sani et al., 2006; Rempfer, 2006; Guermond et al., 2006;  
194 Nordström et al., 2007; Shirokoff and Rosales, 2011; Hosseini and Feng, 2011; Vreman,  
195 2014). Typical fractional-step solution methodologies and associated pressure (or

196 pseudo-pressure) boundary-condition implementations are often verified using various  
197 prototypic flows such as Poiseuille flows, lid-driven cavity flows, flows over cylinders or  
198 bluff bodies, viscously decaying vortices, and dam-break flows. We are unaware of  
199 verification tests in which flows were driven by a heterogeneous surface buoyancy  
200 forcing. Our solution is designed to fill this gap.

201         The analytical solution is derived in Sect. 2. In Sect. 3, this solution is compared  
202 to numerically simulated fields in a steady state. Two versions of a numerical code are  
203 run: a version in which the correct surface pressure boundary condition is applied, and a  
204 version in which the pressure condition is mis-specified. A summary follows in Sect. 4.

205

## 206 **2 Analytical solution**

207 We derive the solution for steady flow over an underlying surface along which the  
208 buoyancy varies laterally as a single harmonic function. This single-harmonic solution is  
209 then used as a building block in a Fourier representation of the square-wave solution.

210

### 211 **2.1 Governing equations**

212 Consider the flow of a viscous stably stratified fluid that fills the semi-infinite domain  
213 above a solid horizontal surface (placed at  $z = 0$ ). This surface undergoes a steady  
214 thermal forcing that varies periodically in the right-hand Cartesian  $x$  direction, but is  
215 independent of the  $y$  direction. The two-dimensional  $(x, z)$  flow is periodic in  $x$ , and

216 satisfies the linearized (assuming the disturbance is of small amplitude) governing  
 217 equations under the Boussinesq approximation,

$$218 \quad 0 = -\frac{\partial \Pi}{\partial x} + \nu \nabla^2 u, \quad (2.1)$$

$$219 \quad 0 = -\frac{\partial \Pi}{\partial z} + b + \nu \nabla^2 w, \quad (2.2)$$

$$220 \quad 0 = -N^2 w + \alpha \nabla^2 b, \quad (2.3)$$

$$221 \quad \frac{\partial u}{\partial x} + \frac{\partial w}{\partial z} = 0. \quad (2.4)$$

222 Apart from notational differences, (2.1)–(2.4) are the two-dimensional steady state  
 223 versions of (55)–(57) of Sect. II of Chandrasekhar (1961). Equations (2.1) and (2.2) are  
 224 the horizontal ( $x$ ) and vertical ( $z$ ) equations of motion, respectively, (2.3) is the thermal  
 225 energy equation (differential form of the first law of thermodynamics) expressed in  
 226 terms of the buoyancy variable (defined below), and (2.4) is the incompressibility  
 227 condition. Here  $u$  and  $w$  are the horizontal and vertical velocity components,  $\Pi \equiv$   
 228  $[p - p_e(z)]/\rho_w$  is the kinematic pressure perturbation [ $p$  is pressure,  $p_e(z)$  is pressure in a  
 229 hydrostatic environmental state in which the density profile is  $\rho_e(z)$ ,  $\rho_w$  is a constant  
 230 reference density, say,  $\rho_e(0)$ ], and  $b \equiv -g[\rho - \rho_e(z)]/\rho_w$  is the buoyancy, where  $\rho$  is the  
 231 actual density, and  $g$  is the acceleration due to gravity. The Brunt-Väisälä frequency  
 232  $N \equiv \sqrt{-(g/\rho_w)d\rho_e/dz}$  of the ambient fluid (Kundu 1990), kinematic viscosity  $\nu$ , and  
 233 thermal diffusivity  $\alpha$  are taken constant.

234 We obtain our solution using a standard vorticity/streamfunction formulation.

235 Cross-differentiating (2.1) and (2.2) yields the vorticity equation,

$$236 \quad 0 = -\frac{\partial b}{\partial x} + \nu \nabla^2 \eta, \quad (2.5)$$

237 where  $\eta \equiv \partial u / \partial z - \partial w / \partial x$  is the vorticity. Eliminating  $b$  from (2.3) and (2.5) yields

$$238 \quad \nabla^4 \eta = \frac{N^2}{\nu \alpha} \frac{\partial w}{\partial x}. \quad (2.6)$$

239 Introducing a streamfunction  $\psi$  defined through

$$240 \quad u = \partial \psi / \partial z, \quad w = -\partial \psi / \partial x, \quad (2.7)$$

241 guarantees that (2.4) is satisfied, and transforms (2.6) into a single equation for  $\psi$ ,

$$242 \quad \nabla^6 \psi + \frac{N^2}{\nu \alpha} \frac{\partial^2 \psi}{\partial x^2} = 0. \quad (2.8)$$

243 The dependent variables are assumed to vanish far above the surface ( $z \rightarrow \infty$ ). On the

244 surface we apply no-slip ( $u = 0$ ) and impermeability ( $w = 0$ ) conditions, and specify a

245 periodic (in  $x$ ) buoyancy distribution. As we will now see, restricting the dependent

246 variables to steady periodic forms that vanish as  $z \rightarrow \infty$  also restricts acceptable

247 distributions of the surface buoyancy. The restriction was first noted by Egger (1981,

248 Sect. 3c), though without details. Averaging (2.3) over one period (using  $w = -\partial \psi / \partial x$ )

249 yields  $d^2 \bar{b} / dz^2 = 0$ , which integrates to  $\bar{b} = A + Bz$  ( $\bar{b}$  is the average of  $b$ ;  $A$  and  $B$  are

250 constants). Taking  $b \rightarrow 0$  as  $z \rightarrow \infty$ , implies that  $\bar{b} \rightarrow 0$  as  $z \rightarrow \infty$ , in which case  $A =$

251  $B = 0$ , and  $\bar{b}(z) = 0$ . In particular, at the surface,  $\bar{b}(0) = 0$ . If a surface distribution

252  $b(x,0)$  violates this condition, the ground acts as a net heat source/sink. In an unsteady  
 253 model, such a source/sink would force a continually upward-developing disturbance, and  
 254 a steady state could never be attained.

255

## 256 2.2 Single-harmonic forcing

257 For a surface buoyancy of the form  $b(x,0) \propto \sin kx$ , (2.3) indicates that  $\psi$  is of the form

$$258 \quad \psi = A(z) \cos kx. \quad (2.9)$$

259 Application of (2.9) in (2.8) yields

$$260 \quad \left( \frac{d^2}{dz^2} - k^2 \right)^3 A - \frac{N^2 k^2}{\nu \alpha} A = 0, \quad (2.10)$$

261 which has solutions of the form  $A \propto e^{Mz}$  for  $M$  satisfying

$$262 \quad (M^2 - k^2)^3 = \frac{N^2 k^2}{\nu \alpha}. \quad (2.11)$$

263 Taking the one-third power of (2.11) yields a useful intermediate result:

$$264 \quad M^2 - k^2 = \frac{N^{2/3} k^{2/3}}{\nu^{1/3} \alpha^{1/3}} e^{2n\pi i/3}, \quad (2.12)$$

265 where  $n$  is an integer. Rearranging (2.12) and taking the square root yields

$$266 \quad M = \pm \sqrt{k^2 + \frac{N^{2/3} k^{2/3}}{\nu^{1/3} \alpha^{1/3}} e^{2n\pi i/3}}. \quad (2.13)$$

267 Equation (2.13) furnishes six roots, two for each of  $n = 0, 1, 2$ . To ensure that  $A(z) \rightarrow 0$

268 as  $z \rightarrow \infty$ , we reject the roots with a positive real part. With the radicand of (2.13)

269 expressed in polar form, the physically acceptable roots are

$$270 \quad M_0 = -\sqrt{k^2 + \frac{N^{2/3}k^{2/3}}{\nu^{1/3}\alpha^{1/3}}}, \quad (n = 0), \quad (2.14a)$$

$$271 \quad M_1 = -r^{1/2}e^{i\phi/2}, \quad (n = 1), \quad (2.14b)$$

$$272 \quad M_2 = -r^{1/2}e^{-i\phi/2}, \quad (n = 2), \quad (2.14c)$$

273 where the subscript on  $M$  denotes the associated value of  $n$ , and  $r$  and  $\phi$  are defined by

$$274 \quad r \equiv \sqrt{\left[ k^2 + \frac{N^{2/3}k^{2/3}}{\nu^{1/3}\alpha^{1/3}} \cos\left(\frac{2\pi}{3}\right) \right]^2 + \left[ \frac{N^{2/3}k^{2/3}}{\nu^{1/3}\alpha^{1/3}} \sin\left(\frac{2\pi}{3}\right) \right]^2}, \quad (2.15)$$

$$275 \quad \cos \phi = \frac{1}{r} \left[ k^2 + \frac{N^{2/3}k^{2/3}}{\nu^{1/3}\alpha^{1/3}} \cos\left(\frac{2\pi}{3}\right) \right], \quad \sin \phi = \frac{1}{r} \left( \frac{N^{2/3}k^{2/3}}{\nu^{1/3}\alpha^{1/3}} \right) \sin\left(\frac{2\pi}{3}\right) > 0. \quad (2.16)$$

276 While solving (2.16) for  $\phi$ , care must be taken when evaluating arcsin or arccos

277 functions that  $\phi$  appears in the correct quadrant ( $\phi$  should be in quadrant I or II so

278  $\phi/2$  should always be in quadrant I). Also note from (2.14b) and (2.14c) that  $M_2$  is the

279 complex conjugate of  $M_1$  ( $M_2 = M_1^*$ ), a fact that will often be used below.

280 With the general solution for  $\psi$  written as

$$281 \quad \psi = (B e^{M_0 z} + C e^{M_1 z} + D e^{M_2 z}) \cos kx, \quad (2.17)$$

282 where  $B$ ,  $C$ , and  $D$  are constants, the vorticity becomes,

$$283 \quad \eta = \left[ B(M_0^2 - k^2) e^{M_0 z} + C(M_1^2 - k^2) e^{M_1 z} + D(M_2^2 - k^2) e^{M_2 z} \right] \cos kx, \quad (2.18)$$

284 and the buoyancy follows from (2.3) as

285 
$$b = \frac{kN^2}{\alpha} \left( \frac{B}{M_0^2 - k^2} e^{M_0 z} + \frac{C}{M_1^2 - k^2} e^{M_1 z} + \frac{D}{M_2^2 - k^2} e^{M_2 z} \right) \sin kx + b_h, \quad (2.19)$$

286 where  $\nabla^2 b_h = 0$ . In view of (2.12), equation (2.19) becomes

287 
$$b = \frac{k^{1/3} \nu^{1/3} N^{4/3}}{\alpha^{2/3}} (B e^{M_0 z} + e^{-2\pi i/3} C e^{M_1 z} + e^{-4\pi i/3} D e^{M_2 z}) \sin kx + b_h. \quad (2.20)$$

288 Applying (2.18) and (2.20) in (2.5) yields an equation for  $\partial b_h / \partial x$ , which upon use of

289 (2.12) and  $M_2 = M_1^*$  reduces to  $\partial b_h / \partial x = 0$ . So  $b_h$  is, at most, a function of  $z$ . Since

290  $\nabla^2 b_h = 0$ ,  $b_h$  is, at most, a linear function of  $z$ , and since  $b$  should vanish as  $z \rightarrow \infty$ ,

291 that linear function must be 0. Thus,  $b_h = 0$ .

292 The pressure follows from (2.1) and (2.12) as

293 
$$\Pi = \frac{\nu^{2/3} N^{2/3}}{k^{1/3} \alpha^{1/3}} (B M_0 e^{M_0 z} + C M_1 e^{2\pi i/3} e^{M_1 z} + D M_2 e^{4\pi i/3} e^{M_2 z}) \sin kx + G(z), \quad (2.21)$$

294 where  $G(z)$  is a function of integration. Applying (2.21) in (2.2), and using (2.11) yields

295  $dG/dz = 0$ , so  $G$  is constant. For  $\Pi$  to vanish as  $z \rightarrow \infty$ , this constant must be zero.

296 The surface conditions determine  $B$ ,  $C$ , and  $D$ . The surface buoyancy is

297 
$$b(x, 0) = b_0 \sin kx, \quad (2.22)$$

298 where  $b_0$  is a constant forcing amplitude. Application of (2.20) in (2.22) yields

299 
$$B + e^{-2\pi i/3} C + e^{-4\pi i/3} D = \frac{b_0 \alpha^{2/3}}{k^{1/3} \nu^{1/3} N^{4/3}}. \quad (2.23)$$

300 In view of (2.7) and (2.17), the impermeability condition  $w(x, 0) = 0$  and no-slip



301 condition  $u(x,0) = 0$  yield

$$302 \quad B + C + D = 0, \quad (2.24)$$

$$303 \quad BM_0 + CM_1 + DM_2 = 0. \quad (2.25)$$

304 Straightforward but lengthy manipulations yield the solution of (2.23)–(2.25):

$$305 \quad B = - \left( \frac{b_0 \alpha^{2/3}}{\sqrt{3} k^{1/3} \nu^{1/3} N^{4/3}} \right) \frac{2r^{1/2} \sin(\phi/2)}{M_0 + 2r^{1/2} \cos(\pi/3 + \phi/2)}, \quad (2.26)$$

$$306 \quad C = -i \left( \frac{b_0 \alpha^{2/3}}{\sqrt{3} k^{1/3} \nu^{1/3} N^{4/3}} \right) \frac{M_2 - M_0}{M_0 + 2r^{1/2} \cos(\pi/3 + \phi/2)}, \quad (2.27)$$

$$307 \quad D = i \left( \frac{b_0 \alpha^{2/3}}{\sqrt{3} k^{1/3} \nu^{1/3} N^{4/3}} \right) \frac{M_1 - M_0}{M_0 + 2r^{1/2} \cos(\pi/3 + \phi/2)}. \quad (2.28)$$

308 Applying (2.26)–(2.28) in (2.17), (2.20), and (2.18), with (2.12) used in the latter  
 309 equation, and noting that  $B$  is real, while  $D = C^*$  (since  $M_2 = M_1^*$ ), we obtain

$$310 \quad b = \frac{2b_0}{\sqrt{3}} \frac{e^{-Z_c} [\mu \cos(Z_s + \pi/6) + \cos(Z_s + \pi/6 + \phi/2)] - e^{M_0 z} \sin(\phi/2)}{\mu + 2 \cos(\pi/3 + \phi/2)} \sin kx, \quad (2.29)$$

$$311 \quad \psi = \frac{2b_0 \alpha^{2/3}}{\sqrt{3} k^{1/3} \nu^{1/3} N^{4/3}} \frac{e^{-Z_c} [\mu \sin Z_s + \sin(Z_s + \phi/2)] - e^{M_0 z} \sin(\phi/2)}{\mu + 2 \cos(\pi/3 + \phi/2)} \cos kx, \quad (2.30)$$

312 where

$$313 \quad Z_s \equiv z r^{1/2} \sin(\phi/2), \quad Z_c \equiv z r^{1/2} \cos(\phi/2), \quad \mu \equiv M_0 / r^{1/2}. \quad (2.31)$$

314 Application of (2.30) in (2.7) yields the velocity components as

315 
$$u = \frac{2b_0 \alpha^{2/3} r^{1/2}}{\sqrt{3} k^{1/3} \nu^{1/3} N^{4/3}} \frac{e^{-Z_c} [\mu \sin(\phi/2 - Z_s) - \sin Z_s] - \mu e^{M_0 z} \sin(\phi/2)}{\mu + 2 \cos(\pi/3 + \phi/2)} \cos kx \quad (2.32)$$

316 
$$w = \frac{2b_0 \alpha^{2/3} k^{2/3}}{\sqrt{3} \nu^{1/3} N^{4/3}} \frac{e^{-Z_c} [\mu \sin Z_s + \sin(Z_s + \phi/2)] - e^{M_0 z} \sin(\phi/2)}{\mu + 2 \cos(\pi/3 + \phi/2)} \sin kx. \quad (2.33)$$

317

### 318 2.3 Piecewise constant (square wave) forcing

319 Next, consider the case where the surface buoyancy varies horizontally as a square

320 wave, with a distribution over one period  $L$  given by

321 
$$b(x, 0) = \begin{cases} b_{\max}, & 0 < x < L/2, \\ -b_{\max}, & L/2 < x < L. \end{cases} \quad (2.34)$$

322 Such a distribution can be expressed as the Fourier series:

323 
$$b(x, 0) = \sum_{n=1}^{\infty} b_n \sin\left(\frac{n\pi x}{L}\right), \quad (2.35)$$

324 
$$b_n = \frac{2}{L} \int_0^L b(x, 0) \sin\left(\frac{n\pi x}{L}\right) dx. \quad (2.36)$$

325 Application of (2.34) in (2.36) yields

326 
$$b_n = \frac{2b_{\max}}{n\pi} [1 - 2 \cos(n\pi/2) + \cos(n\pi)]. \quad (2.37)$$

327 The solutions for  $b$ ,  $\psi$ ,  $u$ , and  $w$  can then be written as summations over the single-

328 harmonic solutions (2.29), (2.30), (2.32), and (2.33), with  $k$  related to  $n$  by

329 
$$k = \frac{n\pi}{L}, \quad (2.38)$$

330 and with  $b_0$  replaced by  $b_n$  :

$$331 \quad b = \frac{2}{\sqrt{3}} \sum_{n=1}^{\infty} b_n \frac{e^{-Z_c} [\mu \cos(Z_s + \pi/6) + \cos(Z_s + \pi/6 + \phi/2)] - e^{M_0 z} \sin(\phi/2)}{\mu + 2 \cos(\pi/3 + \phi/2)} \sin\left(\frac{n\pi x}{L}\right), \quad (2.39)$$

$$332 \quad \psi = \frac{2\alpha^{2/3}}{\sqrt{3} \nu^{1/3} N^{4/3}} \sum_{n=1}^{\infty} \frac{b_n}{k^{1/3}} \frac{e^{-Z_c} [\mu \sin Z_s + \sin(Z_s + \phi/2)] - e^{M_0 z} \sin(\phi/2)}{\mu + 2 \cos(\pi/3 + \phi/2)} \cos\left(\frac{n\pi x}{L}\right), \quad (2.40)$$

$$333 \quad u = \frac{2\alpha^{2/3}}{\sqrt{3} \nu^{1/3} N^{4/3}} \sum_{n=1}^{\infty} b_n \frac{r^{1/2}}{k^{1/3}} \frac{e^{-Z_c} [\mu \sin(\phi/2 - Z_s) - \sin Z_s] - \mu e^{M_0 z} \sin(\phi/2)}{\mu + 2 \cos(\pi/3 + \phi/2)} \cos\left(\frac{n\pi x}{L}\right), \quad (2.41)$$

$$334 \quad w = \frac{2\alpha^{2/3}}{\sqrt{3} \nu^{1/3} N^{4/3}} \sum_{n=1}^{\infty} b_n k^{2/3} \frac{e^{-Z_c} [\mu \sin Z_s + \sin(Z_s + \phi/2)] - e^{M_0 z} \sin(\phi/2)}{\mu + 2 \cos(\pi/3 + \phi/2)} \sin\left(\frac{n\pi x}{L}\right). \quad (2.42)$$

335

### 336 **3 Verification tests**

337 A solution of the linearized equations may be used to verify a nonlinear code if the  
 338 nonlinear terms are sufficiently small. Unfortunately, *a priori* estimates of such terms  
 339 expressed, for example, through a Reynolds number, are not straightforward since the  
 340 relevant velocity and length scales in our problem are only evident after a solution has  
 341 been obtained. We thus seek an appropriate set of test parameters through trial and  
 342 error, guided by *a posteriori* linear solution estimates of the terms  $\mathbf{u} \cdot \nabla b$  and  $\mathbf{u} \cdot \nabla \eta$   
 343 [ $\mathbf{u} = (u, w)$ ] present in nonlinear versions of (2.3) and (2.5), respectively. Specifically, for  
 344 any computed candidate solution, we formed the ratios of the largest values of those  
 345 nonlinear terms to the largest values of the corresponding linear terms, that is, the

346 terms actually present in (2.3) and (2.5). We need only consider one such linear term  
 347 per ratio since (2.3) and (2.5) are comprised of two terms of equal magnitude. A  
 348 solution was deemed to be sufficiently linear if

$$349 \quad R_\eta \equiv \frac{\max|\mathbf{u} \cdot \nabla \eta|}{\max|\partial b / \partial x|} < \varepsilon, \quad \text{and} \quad R_b \equiv \frac{\max|\mathbf{u} \cdot \nabla b|}{\max|\alpha \nabla^2 b|} < \varepsilon, \quad (3.1)$$

350 where  $\varepsilon$  ( $\ll 1$ ) is a prescribed threshold. The suitability of this approach was  
 351 confirmed by the very close agreement between the analytical solutions and the  
 352 numerical solutions obtained with the correct surface pressure condition.

353         The numerical model employed in our tests is a variant of a direct numerical  
 354 simulation (DNS) code used in the boundary-layer and slope-flow studies of Fedorovich  
 355 et al. (2001), Fedorovich and Shapiro (2009a,b), and Shapiro and Fedorovich (2013,  
 356 2014). The model solves the Boussinesq governing equations on a staggered (Arakawa  
 357 C) grid. Although designed for three-dimensional simulations, the model was run in a  
 358 two-dimensional ( $x, z$ ) mode. The overall solution procedure is patterned on a fractional  
 359 step method proposed by Chorin (1968). In our version, the prognostic equations are  
 360 integrated using a filtered leapfrog scheme with explicit treatment of the viscous term.  
 361 The pressure is diagnosed from a Poisson equation (equation (A3b), discussed in the  
 362 Appendix), which is solved using a fast Fourier transform technique in horizontal  
 363 planes, and a tridiagonal matrix inversion in the vertical. The surface condition on  
 364 pressure is the inhomogeneous Neumann condition (INC) that arises from projecting the

365 vertical equation of motion into the vertical, and imposing the impermeability condition  
366 (Vreman, 2014; also see the Appendix). We also run a version of the code in which the  
367 surface pressure condition is mis-specified as a homogeneous Neumann condition (HNC).  
368 We hasten to add, however, that our implementation of the HNC may be quite different  
369 from implementations described in the literature. We elaborate on these technical  
370 differences and review general aspects of the problem of surface pressure specification in  
371 the Appendix.

372 The analytical solution was evaluated on an un-staggered  $(x, z)$  grid extending  
373 over one period of the square wave ( $x = 0$  to  $x = L$ ). The series were truncated at  
374 50000 terms. The governing parameters were adjusted so that the linearity criteria  
375 were satisfied in comparisons with  $\varepsilon = 5 \times 10^{-3}$ .

376 In the first test, we set  $\nu = \alpha = 0.001 \text{ m}^2 \text{ s}^{-1}$ ,  $N = 0.02 \text{ s}^{-1}$ ,  $L = 5.12 \text{ m}$ , and  $b_{\max}$   
377  $= 1 \times 10^{-5} \text{ m s}^{-2}$ . For the analytical solution A-1, the  $(x, z)$  grid consisted of 513 points  
378 in the  $x$  direction and 1025 points in the  $z$  direction, with grid spacings  
379  $\Delta x = \Delta z = 0.01 \text{ m}$ . The linearity criteria (3.1) were satisfied with  $R_\eta \cong 8.2 \times 10^{-5}$  and  
380  $R_b \cong 2.8 \times 10^{-3}$ . The analytical  $b$  and  $w$  fields shown in Fig. 2 depict a broad zone of  
381 ascent above the warm surface and a compensating zone of descent over the cold  
382 surface, roughly for  $z < 1.8 \text{ m}$ . In the upper part of these zones (at roughly  
383  $0.9 \text{ m} < z < 1.8 \text{ m}$ ), adiabatic expansion/compression has reversed the senses of the

384 buoyancy fields. Surprisingly, the numerical fields in the inhomogeneous INC-1 and  
 385 homogeneous HNC-1 cases are very similar to each other and to the A-1 fields. The  $u$   
 386 fields from A-1, INC-1, and HNC-1 shown in Fig. 3 are visually indistinguishable from  
 387 one another.

388 To understand why the INC-1 and HNC-1 simulations are so similar, and to  
 389 identify simulation parameters that might evince more substantial differences, we  
 390 consider the idealized problem in which a specified buoyancy  $b = b_0 e^{-\gamma z} \sin kx$  ( $\gamma = h^{-1}$ ,  
 391 where  $h$  is the e-folding depth scale) is the only forcing term in the Poisson equation  
 392  $\nabla^2 \Pi = \partial b / \partial z$ , with Neumann surface condition  $\partial \Pi / \partial z|_0 = b(x, 0)$ . This idealized  
 393 problem is solved as

$$394 \quad \Pi_{\text{INC}}^* = \frac{b_0}{\gamma^2 - k^2} \left( k e^{-kz} - \gamma e^{-\gamma z} \right) \sin kx. \quad (3.2)$$

395 The corresponding solution obtained with the homogeneous Neumann condition,  
 396  $\partial \Pi / \partial z|_0 = 0$ , is

$$397 \quad \Pi_{\text{HNC}}^* = \frac{b_0}{\gamma^2 - k^2} \left( \frac{\gamma^2}{k} e^{-kz} - \gamma e^{-\gamma z} \right) \sin kx. \quad (3.3)$$

398 The relative error ( $RE$ ) in the vertical pressure gradient force associated with (3.2) and  
 399 (3.3), defined as the local absolute error in that force divided by the local buoyancy, is  
 400 calculated as

401 
$$RE \equiv \left| \frac{\partial \Pi_{\text{INC}}^* / \partial z - \partial \Pi_{\text{HNC}}^* / \partial z}{b} \right| = e^{(a-1)kz}, \quad (3.4)$$

402 where  $a \equiv \gamma/k$ . Written in terms of the depth scale  $h$  and wavelength  $\lambda = 2\pi/k$ ,  $a$  can  
 403 be interpreted as an aspect ratio characterizing the width to depth scales of the  
 404 disturbance,  $a = \lambda/(2\pi h) \propto \lambda\gamma$ . From (3.4) we see that  $RE$  decreases exponentially with  
 405  $z$  for disturbances characterized by small aspect ratios,  $a < 1$  (which we refer to as deep  
 406 disturbances) and increases exponentially with  $z$  for disturbances characterized by large  
 407 aspect ratios,  $a > 1$  (which we refer to as shallow disturbances). The buoyancy in Fig. 2  
 408 is suggestive of  $a < 1$ , which indicates that the first test could be classified as a deep  
 409 (error-forgiving) simulation.

410 The preceding analysis suggests that simulations with shallow thermal  
 411 disturbances ( $a > 1$ ) might yield large differences between cases with inhomogeneous  
 412 and homogeneous Neumann conditions. There did not appear to be a straightforward  
 413 way to increase the effective  $a$  by systematically varying the parameters (e.g., increasing  
 414  $L$  tended to increase the effective  $h$ ), but a set of suitable parameters were identified  
 415 through trial and error and were used as the basis for the second test case.

416 In the second test, we set  $\nu = \alpha = 0.0001 \text{ m}^2 \text{ s}^{-1}$ ,  $N = 0.2 \text{ s}^{-1}$ ,  $L = 10.24 \text{ m}$ , and  
 417  $b_{\text{max}} = 5 \times 10^{-6} \text{ ms}^{-2}$ . The analytical solution A-2 was generated with 2049 points in the  
 418  $x$  direction and 513 points in the  $z$  direction, with grid spacings of  $\Delta x = \Delta z = 0.005 \text{ m}$ .  
 419 The linearity criteria were satisfied with  $R_\eta \cong 4.8 \times 10^{-5}$  and  $R_b \cong 3.8 \times 10^{-3}$ . In

420 contrast to the counter-rotating convection rolls seen in the first test, the analytical  $b$   
421 and  $w$  fields shown in Fig. 4 depict narrow updraft/downdraft pairs straddling the  
422 buoyancy discontinuities. Between the narrow updrafts is a broad region of relatively  
423 weak ascent. The  $w$  and  $b$  fields above the cold surface are mirror images of the fields  
424 above the warm surface. Note the change in the scales of the  $x$  and (especially) the  $z$   
425 axes between Figs. 4 and 2: the low-level thermal disturbance in the second test is much  
426 shallower than the disturbance in the first test (and is suggestive of  $a > 1$ ). In this  
427 second test case we find dramatic differences between the inhomogeneous INC-2 and  
428 homogeneous HNC-2 cases. Specifically, while the INC-2 and A-2 fields are in excellent  
429 agreement, the HNC-2 fields showed no signs of even approaching a steady state. Long  
430 after the INC-2 simulation had reached a steady state, the HNC-2 fields continued to  
431 amplify and develop asymmetric structures associated with flow nonlinearities. The very  
432 close agreement between the A-2 solution and the steady state in the INC-2 simulation  
433 is shown for the  $u$  field in Fig. 5. The  $u$  field in the disastrous HNC-2 simulation, at a  
434 time when a steady state had already been attained in the INC-2 simulation, is shown  
435 in Fig. 6.

436

#### 437 **4 Summary**

438 The linearized Boussinesq equations for the motion of a viscous stably stratified fluid  
439 are solved analytically for a surface buoyancy that varies laterally as a square wave.



440 The solution describes two-dimensional laminar convective structures such as thermal  
441 convective rolls and updraft/downdraft pairs. The main applications of the solution may  
442 be in code verification and the evaluation of different implementations of the surface  
443 pressure condition for the pressure Poisson equation. Tests have been conducted for  
444 cases where the aspect ratios of the thermal disturbance have been large and small.  
445 With attention restricted to disturbances of sufficiently small amplitude, the linear  
446 solution and numerically simulated fields with the inhomogeneous Neumann condition  
447 for pressure (which is appropriate in the context of the particular fractional step  
448 procedure adopted in our DNS code) have been found to be in excellent agreement for  
449 both tests. However, in tests with a mis-specified Neumann condition, an excellent  
450 agreement with the analytical solution has been found only for the deep (small aspect  
451 ratio) disturbance case; errors in the shallow (large aspect ratio) disturbance case have  
452 been catastrophic.

453 **Appendix A: Comment on the pressure condition at a lower solid surface**

454 Consider a three-dimensional Boussinesq system with equation of motion,

455 
$$\frac{\partial \mathbf{u}}{\partial t} = -\nabla \Pi + \nu \nabla^2 \mathbf{u} + \mathbf{F}. \quad (\text{A1})$$

456 Here  $\mathbf{u} = (u, v, w)$  is the three-dimensional velocity vector,  $\Pi$  is a kinematic pressure  
 457 perturbation,  $\nu$  is the kinematic viscosity coefficient, and  $\mathbf{F}$  is the sum of nonlinear  
 458 acceleration and buoyancy terms. Applying the incompressibility condition,

459 
$$\nabla \cdot \mathbf{u} = 0, \quad (\text{A2})$$

460 in the equation that results from taking the divergence of (A1) (e.g., Orszag et al., 1986)  
 461 yields the Poisson equation,

462 
$$\nabla^2 \Pi = \nabla \cdot \mathbf{F}. \quad (\text{A3a})$$

463 Although (A1) and (A2) imply (A3a), the reverse statement is not generally true.  
 464 Indeed, eliminating  $\Pi$  from between (A3a) and the equation arising from taking the  
 465 divergence of (A1) yields the diffusion equation  $\partial \delta / \partial t = \nu \nabla^2 \delta$  for the velocity  
 466 divergence  $\delta \equiv \nabla \cdot \mathbf{u}$ , whose solution is (A2) only if  $\delta$  is zero initially and on all  
 467 boundaries (Orszag et al., 1986; Gresho and Sani, 1987, Vreman 2014).

468 The same steps leading to (A3a) also lead to an alternative Poisson equation,

469 
$$\nabla^2 \Pi = \nabla \cdot (\nu \nabla^2 \mathbf{u} + \mathbf{F}). \quad (\text{A3b})$$

470 Although  $\nabla \cdot \nu \nabla^2 \mathbf{u}$  was omitted in (A3a) [this term is zero if (A2) is satisfied], without  
 471 further constraints on  $\delta$  (described above), (A2) may not be satisfied. Gresho and Sani

472 (1987) showed that the retention of  $\nabla \cdot \nu \nabla^2 \mathbf{u}$  in (A3b) assures that (A2) is satisfied,  
473 and thus leads to the paradox: "If you include it, you don't need it; if you don't include  
474 it, you need it." Vreman (2014) revisited this paradox, and showed that for a standard  
475 staggered method, the discretized form of (A3b) is equivalent to that of (A3a)  
476 supplemented with the constraint that  $\nabla \cdot \nabla^2 \mathbf{u} = 0$  ( $\nabla^2 \delta = 0$ ) on points adjacent to the  
477 solid boundary [with the same inhomogeneous Neumann boundary condition for  $\Pi$   
478 implied for (A3a) and (A3b)]. When supplemented with this  $\nabla^2 \delta = 0$  near-wall  
479 condition, the diffusion equation for  $\delta$  led to  $\delta = 0$  for all time. We note that (A3b) is  
480 the form adopted in our numerical code.

481 Evaluating the vertical component of (A1) on the surface, where the  
482 impermeability condition applies, yields the inhomogeneous Neumann condition,

$$483 \quad \left. \frac{\partial \Pi}{\partial z} \right|_0 = \nu \left. \frac{\partial^2 w}{\partial z^2} \right|_0 + F_z \Big|_0, \quad (\text{A4})$$

484 where  $w \equiv \mathbf{k} \cdot \mathbf{u}$ ,  $F_z \equiv \mathbf{k} \cdot \mathbf{F}$ ,  $\mathbf{k}$  is the upward unit vector, and  $(\ ) \Big|_0$  is a surface value. It  
485 has been argued that (A4), by itself, is not a proper boundary condition because it does  
486 not provide new information (it is not independent of the governing equations) and does  
487 not enforce the incompressibility condition (A2) at the boundary (Strikwerda, 1984;  
488 Henshaw, 1994; Sani et al., 2006). However, as pointed out by Henshaw (1994), many  
489 studies that impose (A4) (or a variant of it) also apply (A2) on the boundary.

490 In our numerical model, (A1) is integrated using a fractional step procedure with

491 explicit treatment of the viscous term. First, a provisional velocity field  $\tilde{\mathbf{u}}$  that does not  
492 satisfy (A2) is obtained by integrating a discretized form of (A1) in which the pressure  
493 gradient is omitted. The provisional velocity is equal to the velocity at the end of the  
494 previous time step plus the sum of the forcing terms (nonlinear acceleration, buoyancy,  
495 and viscous stress) multiplied by the time step  $\Delta t$ . With the forcing terms explicitly  
496 evaluated,  $\tilde{\mathbf{u}}$  is readily computed throughout the flow domain, including on the surface,  
497 where, in surface-forced flows, the buoyancy will make a substantial contribution. In  
498 terms of  $\tilde{\mathbf{u}}$  and its vertical component  $\tilde{w}$ , (A3b) and (A4) become,

$$499 \quad \nabla^2 \Pi = \frac{\nabla \cdot \tilde{\mathbf{u}}}{\Delta t}, \quad (\text{A5})$$

$$500 \quad \left. \frac{\partial \Pi}{\partial z} \right|_0 - \frac{1}{\Delta t} \tilde{w} \Big|_0 = 0. \quad (\text{A6})$$

501 In the second step, a velocity field that does satisfy (A2) is obtained by solving (A5) for  
502  $\Pi$  and then adding the pressure gradient force associated with  $\Pi$  (multiplied by  $\Delta t$ ) to  
503  $\tilde{\mathbf{u}}$ .

504 In some explicit fractional step procedures (including the DNS code used in our  
505 study), the problem of solving (A5) subject to (A6) with  $\tilde{\mathbf{u}}|_0$  evaluated from model data  
506 is replaced by what appears to be an entirely different (but is actually equivalent)  
507 problem: solving (A5) subject to the homogeneous Neumann condition,

$$508 \quad \left. \frac{\partial \Pi}{\partial z} \right|_0 = 0, \quad (\text{A7})$$

509 in concert with  $\tilde{\mathbf{u}}|_0$  being set to 0, obviating the need to calculate  $\tilde{\mathbf{u}}|_0$  from model data.  
 510 It can be shown that  $\tilde{w}|_0$  and the discretized form of  $\partial\Pi/\partial z|_0$  appear in the discretized  
 511 form of (A5) valid half a grid point above the physical surface as  $\partial\Pi/\partial z|_0 - \tilde{w}|_0/\Delta t$ , that  
 512 is, in the same combination as they appear in (A6). Thus, setting  $\tilde{w}|_0$  and  $\partial\Pi/\partial z|_0$  to 0,  
 513 is equivalent to implementing (A6) with the model-computed values of  $\tilde{w}|_0$ : the  
 514 discretized form of (A5) near the surface is the same in either case. Moreover, on the C  
 515 grid, setting the tangential components  $\tilde{u}|_0$  and  $\tilde{v}|_0$  to 0 only affects the values of  $\tilde{u}$  and  
 516  $\tilde{v}$  half a grid point beneath the physical boundary. These values do not appear in the  
 517 discretized form of (A5) at any  $z$ -level, and thus have no bearing on the solution. In  
 518 essence, the errors associated with the conflation of the two physically unjustifiable  
 519 specifications (homogeneous Neumann condition for pressure, and  $\tilde{\mathbf{u}}|_0 = 0$ ) cancel out.

520 The homogeneous Neumann condition for pressure can be the source of confusion  
 521 if the context in which the condition is applied is not made clear: it would be a correct  
 522 condition if  $\tilde{\mathbf{u}}|_0$  is set to zero (per the equivalence described above), but it would be an  
 523 incorrect condition if the explicit model-computed values of  $\tilde{\mathbf{u}}|_0$  are used. In the  
 524 experiments with the mis-specified condition described in Sect. 3, the homogeneous  
 525 condition is imposed in the latter context. Unfortunately, in many numerical model  
 526 descriptions, the nature of the surface pressure condition is left vague, for example, by

527 not indicating whether a Neumann condition is homogeneous or inhomogeneous, or, if a  
528 homogeneous Neumann condition is indicated, not mentioning how  $\tilde{\mathbf{u}}|_0$  is treated.

529 Finally, we note that in fractional step procedures that treat the viscous term  
530 implicitly (e.g., Kim and Moin, 1985; Gresho, 1990; Armfield and Street, 2002;  
531 Guermond et al., 2006, and many others), the homogeneous Neumann condition is often  
532 applied as a surface condition for a Poisson equation, but it is again different from our  
533 implementation described in Sect. 3. In the implicit treatments, the provisional velocity  
534 is obtained as the solution of a boundary value problem ( $\tilde{\mathbf{u}}|_0$  should be specified; often  
535 it is set to 0) in which the relevant Poisson equation resembles (A5) but applies to a  
536 scalar function (sometimes called a pseudo-pressure) that is not the real pressure.  
537 Temam (1991) refers to this scalar as, "... a technical quantity, a mathematical  
538 auxiliary..." and advocates that it should not even be considered as an approximation of  
539 the pressure. Interestingly, in the context of implicit treatments, the homogeneous  
540 Neumann condition on the pseudo-pressure has sometimes been implicated as corrupting  
541 solution accuracy through the development of spurious numerical boundary layers  
542 adjacent to solid boundaries (Gresho, 1990; Guermond et al., 2006; Hosseini and Feng,  
543 2011).

544

#### 545 **Code availability**

546 The Fortran program used to generate output data files from the analytical solution is

547 available as a supplement to this article. That program (square.f) is configured for test  
548 A-1, but can be easily adjusted to run test A-2 or other tests. Running square.f  
549 automatically generates an output file for each dependent variable (e.g., u.dat) as well  
550 as an output file (square.out) that summarizes the test parameters and gives the  
551 computed values of the linearity ratios  $R_\eta$  and  $R_b$  defined in (3.1).

552

553 *Acknowledgements.* This research was supported by the National Science Foundation  
554 under Grant AGS-1359698. Comments by Chiel van Heerwaarden, Juan Pedro Mellado,  
555 Inanc Senocak, and an anonymous reviewer are gratefully acknowledged.

556 **References**

- 557 Armfield, S. and Street, R.: An analysis and comparison of the time accuracy of  
558 fractional-step methods for the Navier-Stokes equations on staggered grids. *Int.*  
559 *J. Numer. Methods Fluids*, 38, 255–282, 2002.
- 560 Atkinson, B.: *Meso-scale Atmospheric Circulations*. Academic Press. 495 pp., 1981.
- 561 Axelsen, S. L., Shapiro, A., and Fedorovich, E.: Analytical solution for katabatic flow  
562 induced by an isolated cold strip. *Environ. Fluid Mech.*, 10, 387–414, 2010.
- 563 Briggs, G. A.: Surface inhomogeneity effects on convective diffusion. *Boundary-Layer*  
564 *Meteorol.*, 45, 117–135, 1988.
- 565 Chandrasekhar, S.: *Hydrodynamic and Hydromagnetic Stability*. Oxford University  
566 Press. 652 pp., 1961.
- 567 Chorin, A. J.: Numerical solution of the Navier-Stokes equations. *Math. Comput.*, 22,  
568 745–762, 1968.
- 569 Egger, J.: On the linear two-dimensional theory of thermally induced slope winds. *Beitr.*  
570 *Phys. Atmosph.*, 54, 465–481, 1981.
- 571 Fedorovich, E., Nieuwstadt, F. T. M., and Kaiser, R.: Numerical and laboratory study  
572 of a horizontally evolving convective boundary layer. Part I: Transition  
573 regimes and development of the mixed layer. *J. Atmos. Sci.*, 58, 70–86, 2001.
- 574 Fedorovich, E. and Shapiro, A.: Structure of numerically simulated katabatic and  
575 anabatic flows along steep slopes. *Acta Geophys.*, 57, 981–1010, 2009a.



576 Fedorovich, E. and Shapiro, A.: Turbulent natural convection along a vertical plate  
577 immersed in a stably stratified fluid. *J. Fluid Mech.*, 636, 41–57, 2009b.

578 Gresho, P. M. and Sani, R. L.: On pressure boundary conditions for the incompressible  
579 Navier-Stokes equations. *Int. J. Numer. Methods Fluids*, 7, 1111–1145, 1987.

580 Gresho, P. M.: On the theory of semi-implicit projection methods for viscous  
581 incompressible flow and its implementation via a finite element method that also  
582 introduces a nearly consistent mass matrix. Part 1: Theory. *Int. J. Numer.*  
583 *Methods Fluids*, 11, 587–620, 1990.

584 Guermond, J. L., Mineev, P., and Shen, J.: An overview of projection methods for  
585 incompressible flows. *Comput. Methods Appl. Mech. Engrg.* 195, 6011–6045,  
586 2006.

587 Hadfield, M. G., Cotton, W. R., and Pielke, R. A.: Large-eddy simulations of thermally  
588 forced circulations in the convective boundary layer. Part I: A small-scale  
589 circulation with zero wind. *Boundary-Layer Meteorol.*, 57, 79–114, 1991.

590 Henshaw, W. D: A fourth-order accurate method for the incompressible Navier-Stokes  
591 equations on overlapping grids. *J. Comput. Phys.*, 113, 13–25, 1994.

592 Hosseini, S. M. and Feng, J. J.: Pressure boundary conditions for computing  
593 incompressible flows with SPH. *J. Comput. Phys.*, 230, 7473–7487, 2011.

594 Kang, S.-L., Lenschow, D., and Sullivan, P.: Effects of mesoscale surface thermal  
595 heterogeneity on low-level horizontal wind speeds. *Boundary-Layer Meteorol.*,

596 143, 409–432, 2012.

597 Kim, J. and Moin, P.: Application of a fractional-step method to incompressible  
598 Navier-Stokes equations. *J. Comput. Phys.*, 59, 308–323, 1985.

599 Kundu, P. K.: *Fluid Mechanics*. Academic Press. 638 pp., 1990.

600 Mahrt, L., Sun, J., Vickers, D., MacPherson, J. I., Pederson, J. R., and Desjardins, R.  
601 L.: Observations of fluxes and inland breezes over a heterogeneous surface. *J.*  
602 *Atmos. Sci.*, 51, 2484–2499, 1994.

603 McPherson, R. A.: A review of vegetation-atmosphere interactions and their influences  
604 on mesoscale phenomena. *Prog. Phys. Geog.*, 31, 261–285, 2007.

605 Nordström, J., Mattsson, K., and Swanson, C.: Boundary conditions for a divergence  
606 free velocity-pressure formulation of the Navier-Stokes equations. *J.*  
607 *Comput. Phys.*, 225, 874–890, 2007.

608 Orszag, S. A., Israeli, M., and Deville, M. O.: Boundary conditions for incompressible  
609 flows. *J. Sci. Comput.*, 1, 75–111, 1986.

610 Patton, E. G., Sullivan, P. P., and Moeng, C.-H.: The influence of idealized  
611 heterogeneity on wet and dry planetary boundary layers coupled to the land  
612 surface. *J. Atmos. Sci.*, 62, 2078–2097, 2005.

613 Petersson, N. A.: Stability of pressure boundary conditions for Stokes and Navier-  
614 Stokes equations. *J. Comput. Phys.*, 172, 40–70, 2001.

615 Pielke, R. A.: Influence of the spatial distribution of vegetation and soils on the

616 prediction of cumulus convective rainfall. *Rev. Geophys.*, 39, 151–177, 2001.

617 Rempfer, D.: On boundary conditions for incompressible Navier-Stokes problems. *Appl.*  
618 *Mech. Rev.*, 59, 107–125, 2006.

619 Segal, M. and Arritt, R. W.: Non-classical mesoscale circulations caused by surface  
620 sensible heat-flux gradients. *Bull. Amer. Meteorol. Soc.*, 73, 1593–1604, 1992.

621 Shirokoff, D. and Rosales, R. R.: An efficient method for the incompressible Navier-  
622 Stokes equations on irregular domains with no-slip boundary conditions, high  
623 order up to the boundary. *J. Comput. Phys.*, 230, 8619–8646, 2011.

624 Shapiro, A. and Fedorovich, E.: Similarity models for unsteady free convection flows  
625 along a differentially cooled horizontal surface. *J. Fluid Mech.*, 736, 444–463,  
626 2013.

627 Shapiro, A. and Fedorovich, E.: A boundary-layer scaling for turbulent katabatic flow.  
628 *Boundary-Layer Meteorol.*, 153, 1–17, 2014.

629 Simpson, J. E.: *Sea Breeze and Local Winds*. Cambridge University Press. 234 pp.,  
630 1994.

631 Temam, R.: Remark on the pressure boundary condition for the projection method.  
632 *Theoret. Comput. Fluid Dynamics*, 3, 181–184, 1991.

633 Strikwerda, J. C.: Finite difference methods for the Stokes and Navier-Stokes equations.  
634 *SIAM J. Sci. Stat. Comput.*, 5, 56–68, 1984.

635 van Heerwaarden, C. C., Mellado, J. P., and de Lozar, A.: Scaling laws for the

636 heterogeneously heated free convective boundary layer. *J. Atmos. Sci.*, 71, 3975–  
637 4000, 2014.

638 Vreman, A. W.: The projection method for the incompressible Navier-Stokes equations:  
639 The pressure near a no-slip wall. *J. Comput. Phys.*, 263, 353–374, 2014.

640

641

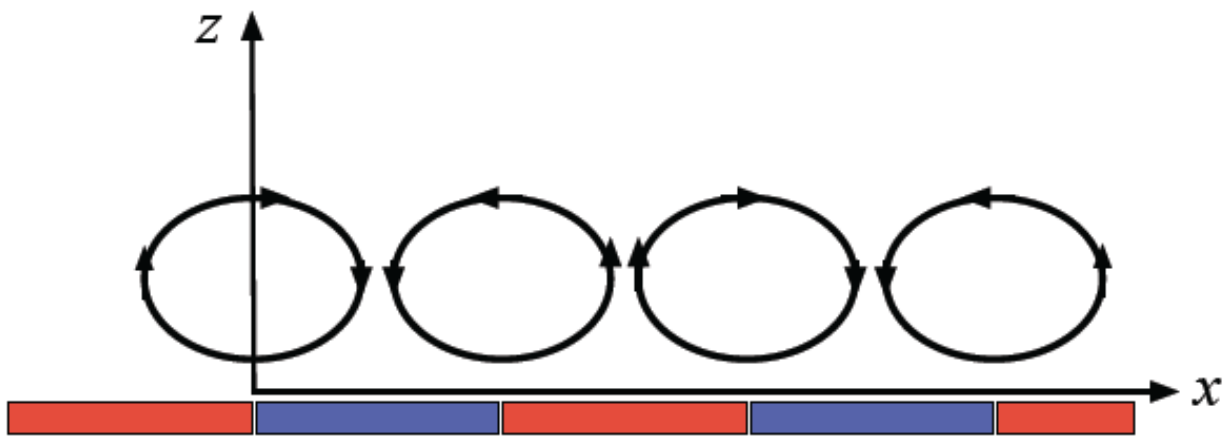
642

643

644

645

646



647

648

649 **Figure 1.** Schematic of two-dimensional  $(x, z)$  thermal convection induced by a surface

650 buoyancy that varies horizontally ( $x$ ) as a square wave. Red denotes positive surface

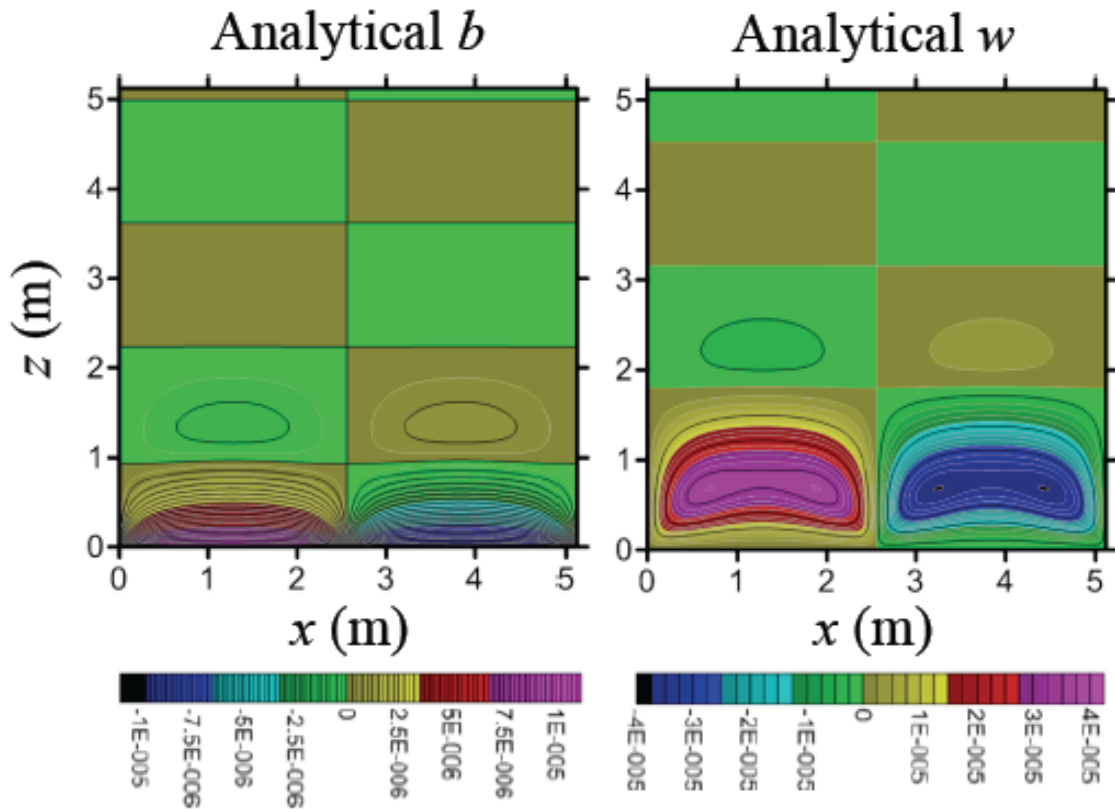
651 buoyancy, blue denotes negative surface buoyancy.

652

653

654

655



656

657

658

659 **Figure 2.** Vertical cross section of the analytical (A-1) buoyancy  $b$  and vertical velocity

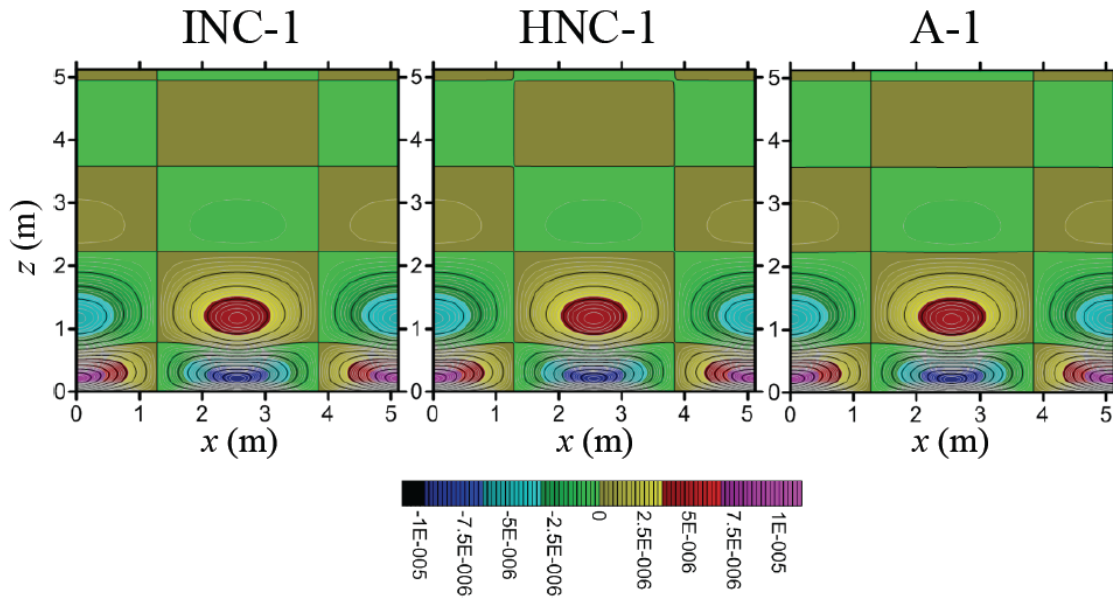
660  $w$  fields from the first test case. Color bar units are  $\text{m s}^{-2}$  for  $b$ , and  $\text{m s}^{-1}$  for  $w$ .

661

662

663

664



665

666

667

668 **Figure 3.** Vertical cross section of  $u$  from the first test case. A-1 is the analytical

669 solution. INC-1 is the numerical simulation with inhomogeneous Neumann condition for

670 pressure. HNC-1 is the numerical simulation with the homogeneous Neumann condition

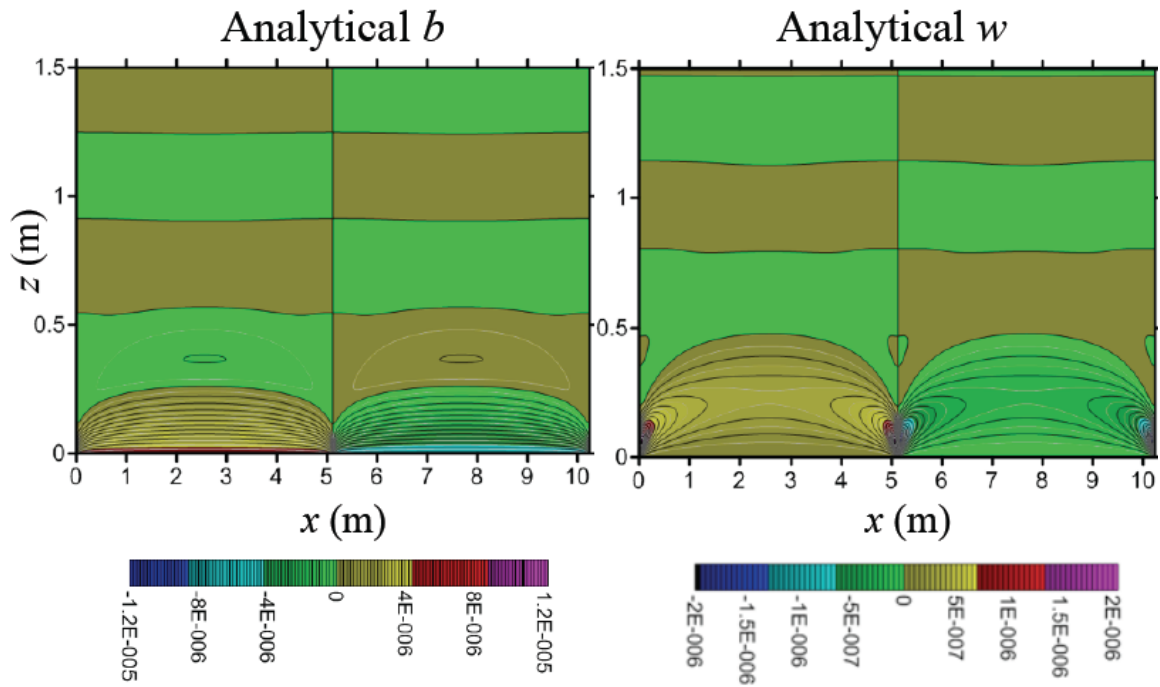
671 for pressure. Color bar units are  $\text{m s}^{-1}$ .

672

673

674

675



676

677

678

679 **Figure 4.** Vertical cross section of the analytical (A-2) buoyancy  $b$  and vertical velocity

680  $w$  fields from the second test case. Color bar units are  $\text{m s}^{-2}$  for  $b$ , and  $\text{m s}^{-1}$  for  $w$ .

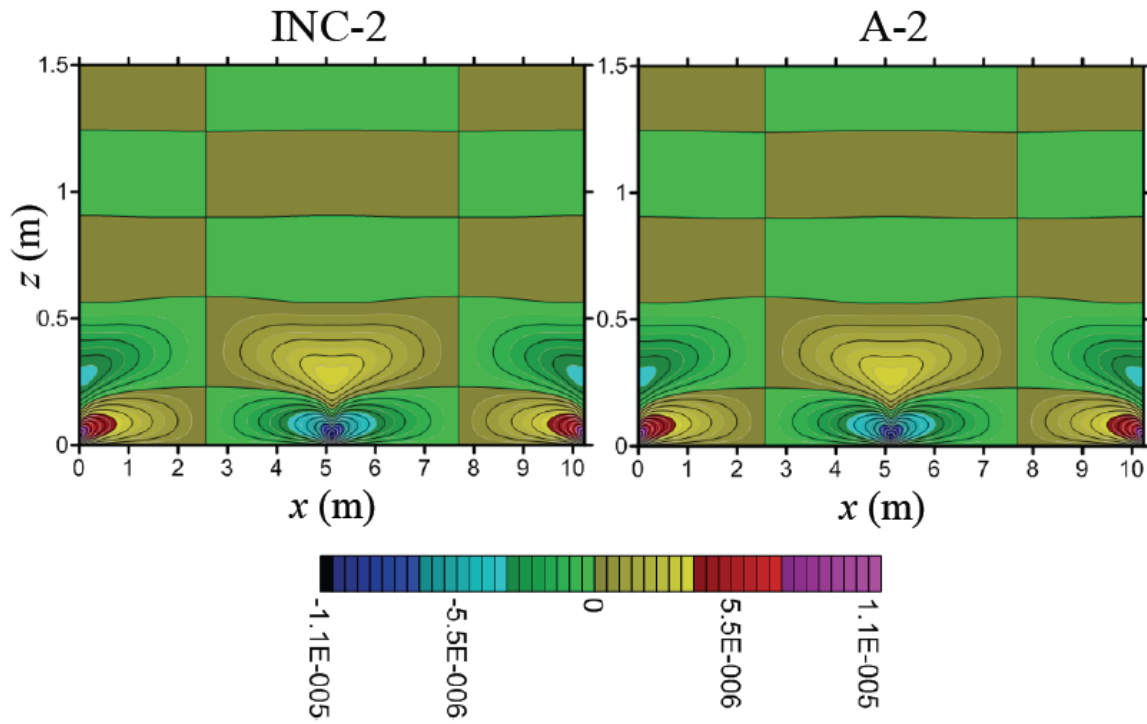
681



682

683

684



685

686

687 **Figure 5.** Vertical cross section of  $u$  from the second test case. A-2 is the analytical

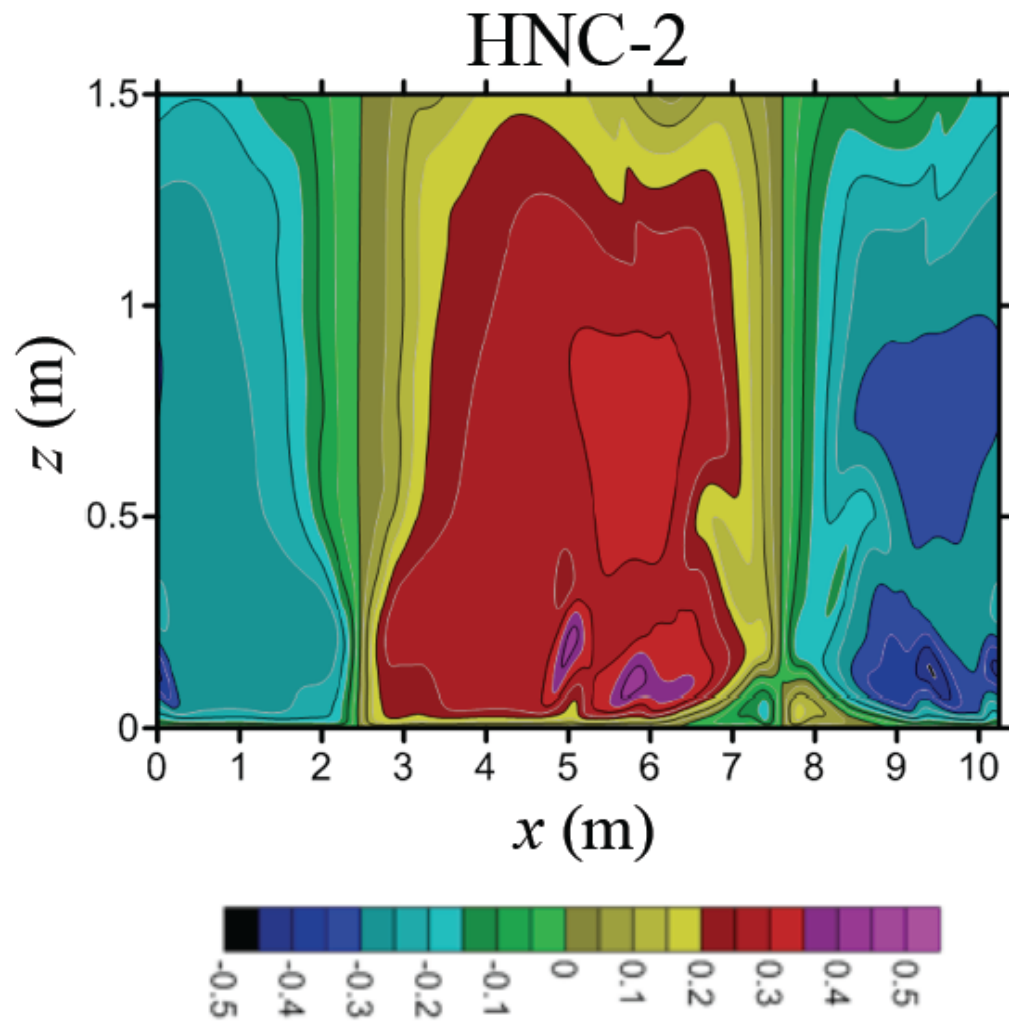
688 solution. INC-2 is the numerical simulation with inhomogeneous Neumann condition for

689 pressure. Color bar units are  $\text{m s}^{-1}$ .

690

691

692



693

694

695 **Figure 6.** Vertical cross section of  $u$  from HNC-2, the numerical simulation with

696 homogeneous Neumann condition for pressure in the second test case. Color bar units

697 are  $\text{m s}^{-1}$ .